

Theoretical Models of Polarized Dust Emission from Protostellar Cores

Paolo Padoan,¹ Alyssa Goodman,
Harvard-Smithsonian Center for Astrophysics, Cambridge, MA 02138

Bruce Draine,
Princeton University Observatory, Peyton Hall, Princeton, NJ 08544

Mika Juvela,
Helsinki University Observatory, Tähtitorninmäki, P.O.Box 14, SF-00014 University of Helsinki, Finland

Åke Nordlund
Copenhagen Astronomical Observatory, and Theoretical Astrophysics Center, 2100 Copenhagen, Denmark

Örnólfur Einar Rögnvaldsson
Nordic Institute for Theoretical Physics, 2100 Copenhagen, Denmark

ABSTRACT

We model the polarized thermal dust emission from protostellar cores that are assembled by super-sonic turbulent flows in molecular clouds.

Self-gravitating cores are selected from a three dimensional simulation of super-sonic and super-Alfvénic magneto-hydrodynamic (MHD) turbulence. The polarization is computed in two ways. In model *A* it is assumed that dust properties and grain alignment efficiency are uniform; in model *B* it is assumed that grains are not aligned at visual extinction larger than $A_{V,0} = 3$ mag, consistent with theoretical expectations for grain alignment mechanisms. Instead of using a specific set of grain properties, we adopt a maximum degree of polarization $P_{max} = 15$ %. Results are therefore sensitive mainly to the topology of the magnetic field (model *A*) and to the gas distribution that determines the distribution of A_V (model *B*). Furthermore, the radiative transfer in the MHD model is solved with a non-LTE Monte Carlo method, to compute spectral maps of the J=1–0 transition of CS. The CS spectral maps are used to estimate the turbulent velocity, as in the observations.

The main results of this work are: i) Values of P between 1 and 10% (up to almost P_{max}) are typical, despite the super-Alfvénic nature of the turbulence; ii) A steep decrease of P with increasing values of the sub-mm dust continuum intensity I is always found in self-gravitating cores selected from the MHD simulations, if grains are not aligned above a certain value of visual extinction $A_{V,0}$ (model *B*); iii) The same behavior is hard to reproduce if grains are aligned independently of A_V (model *A*); iv) The Chandrasekhar-Fermi formula, corrected by a factor $f \approx 0.4$, provides an approximate estimate of the average magnetic field strength in the cores.

Sub-mm dust continuum polarization maps of quiescent protostellar cores and Bok globules have recently been obtained. They always show a decrease in P with increasing value of I consistent with the predictions of our model *B*. We therefore conclude that sub-mm polarization maps of quiescent cores do not map the magnetic field inside the cores at visual extinction larger than $A_{V,0} \approx 3$ mag. The use of such maps to constrain models of protostellar core formation and evolution is questionable. This conclusion suggests that there is no inconsistency between the results from optical and near-IR polarized absorption of background stars, and the observed

¹ppadoan@cfa.harvard.edu

polarization of sub-mm dust continuum from quiescent cores. In both cases, grains at large visual extinction appear to be virtually unaligned.

Subject headings: turbulence – ISM: kinematics and dynamics – radio astronomy: interstellar: dust continuum, polarization and lines

1. Introduction

The topology of the magnetic field inside and around protostellar cores can be predicted with models for their formation and evolution. Models of sub-critical cores contracting under the effect of gravity and ambipolar drift, for example, predict a rather uniform magnetic field roughly perpendicular to the core major axis. Such models can be tested if the magnetic field topology is constrained observationally.

Polarization maps of sub-mm thermal dust emission have recently been obtained for a number of protostellar cores and Bok globules (Minchin, Bonifacio & Murray 1996; Glenn, Walker & Young 1999; Greaves et al. 1999; Coppin et al. 2000; Davis et al. 2000; Matthews & Wilson 2000; Vallée, Bastien & Greaves 2000; Ward-Thompson et al. 2000; Henning et al. 2001). Results are still sparse, but are readily used to try to test theoretical models of core formation and evolution (Glenn, Walker & Young 1999; Coppin et al. 2000; Davis et al. 2000; Ward-Thompson et al. 2000). Since the interpretation of the observations is hardly unique, it is useful to compute polarization maps of the theoretical models, where the full three-dimensional information is available, and to infer their observable properties. Theoretical polarization maps have been previously computed by Wardle & Königl (1990) for the molecular disk at the Galactic center and by Fiege & Pudritz (2000) for molecular cloud filaments.

In this work we assume that protostellar cores are assembled by super-sonic turbulent flows in molecular clouds. We have shown in a previous work that the formation of cores by turbulent shocks provides an excellent interpretation of the relation between integrated intensity and rms velocity in molecular clouds (Padoan et al. 2001). Alternative interpretations of this newly discovered property of molecular clouds have not been proposed so far. Furthermore, super-sonic turbulence is ubiquitously observed in molecular clouds, and therefore models of core formation and evolution must take into account this turbulent environment self-consistently. We do so by selecting self-gravitating cores from a numerical simulation of super-sonic, super-Alfvénic, self-gravitating magneto-hydrodynamic (MHD) turbulence. The simulation is intended to represent a molecular cloud region with size $L = 6.25$ pc, rms turbulent velocity $\sigma_v = 3.0$ km/s and average gas density $\langle n \rangle = 320$ cm⁻³. These are typical values for molecular clouds according to Larson’s relations (Larson 1981). The three selected cores have a mass of $\approx 60 M_\odot$ and a maximum gas density $\sim 10^5$ cm⁻³.

The polarized thermal dust emission is computed in two ways. In model A it is assumed that dust properties and grain alignment efficiency are uniform; in model B it is assumed that grains are not aligned at visual extinction larger than $A_{V,0} = 3$ mag, in line with theoretical expectations for grain alignment mechanisms (Lazarian, Goodman & Meyers 1997). Instead of using a specific set of grain properties, we adopt a maximum degree of polarization $P_{max} = 15$ %. Results are therefore sensitive mainly to the topology of the magnetic field (model A) and to the gas distribution that determines the distribution of A_V (model B). A Monte Carlo method is used to compute the distribution of A_V in the MHD model.

We find that despite the relatively weak magnetic field averaged over the whole computational box, $\langle B \rangle = 3.3$ μ G and $\langle B^2 \rangle^{1/2} = 7.1$ μ G, the degree of polarization is typically between 1 and 10% (as observed), spanning a range of values almost up to P_{max} . In protostellar cores (Davis et al. 2000) and

Bok globules (Henning et al. 2000), P is always found to decrease with increasing sub-mm dust continuum intensity I . This is consistent with our MHD model only if grains are not aligned above a certain value of the visual extinction, $A_{V,0}$ (model B), in agreement with previous results from optical and near-IR polarized absorption of background stars (Goodman et al. 1995; Gerakines et al. 1995; Arce et al. 1998).

We also solve the radiative transfer in the MHD model with a non-LTE Monte Carlo method, to compute spectral maps of the J=1–0 transition of CS. We use these maps to estimate the turbulent velocity dispersion in the same way as in the observations. This turbulent velocity dispersion is used, together with the dispersion in the polarization angle, to infer the magnetic field strength using the Chandrasekhar–Fermi formula (Chandrasekhar & Fermi 1953). It is found that the volume-averaged three dimensional magnetic field strength can be estimated, despite the large dispersion in the polarization angle, if the Chandrasekhar–Fermi formula is used with a coefficient $f \approx 0.4$.

The polarization properties of turbulent molecular clouds depend on the average magnetic field strength, relative to the kinetic energy of turbulence, as measured by the rms Alfvénic Mach number, \mathcal{M}_a , that is the ratio of the rms flow velocity and the Alfvén velocity, (Clemens et al. 2000; Ostriker, Stone & Gammie 2001). A complete statistical study of the polarization properties of turbulent clouds with different values of \mathcal{M}_a will be presented separately, and will be more useful in the future, when a larger number of polarization maps of sub-mm and far-IR dust emission will be available (especially if future satellite missions of the type of M4 (Clemens et al. 2000) will be dedicated to this purpose). In the present work we focus on the properties of a few cores, to provide insight in the interpretation of recent sub-mm observations.

The MHD models are presented in the next section, while in § 3 we describe the method for computing the polarized dust emission. The selection of self-gravitating cores from the synthetic continuum map is discussed in § 4 and the observational results are summarized in § 5. In § 6 the Chandrasekhar–Fermi formula is tested on the selected cores. Results are discussed in § 7, and conclusions are summarized in § 8.

2. The MHD Model

We solve the compressible MHD equations:

$$\frac{\partial \ln \rho}{\partial t} + \mathbf{v} \cdot \nabla \ln \rho = -\nabla \cdot \mathbf{v}, \quad (1)$$

$$\frac{\partial \mathbf{v}}{\partial t} + \mathbf{v} \cdot \nabla \mathbf{v} = -\frac{P}{\rho} \nabla \ln P + \frac{1}{\rho} \mathbf{j} \times \mathbf{B} - \nabla \Phi + \mathbf{f}, \quad (2)$$

$$P = \rho T, \quad (3)$$

$$\frac{\partial \mathbf{B}}{\partial t} = \nabla \times (\mathbf{v} \times \mathbf{B}), \quad (4)$$

$$\mathbf{j} = \nabla \times \mathbf{B}, \quad (5)$$

$$\nabla^2 \Phi = C \rho \quad (6)$$

plus numerical diffusion terms, and with periodic boundary conditions. \mathbf{v} is the velocity, \mathbf{B} the magnetic field, Φ the gravitational potential, \mathbf{f} an external random force, T the gas temperature and $T = \text{const}$ is assumed. The isothermal approximation is appropriate for the short cooling time in relatively dense molecular gas (see discussion in Padoan, Zweibel & Nordlund 2000). The constant C is given by:

$$C = \frac{4\pi G l_0^2 \rho_0}{v_0^2}, \quad (7)$$

where the velocity is measured in units of v_0 , length in units of l_0 , time in units of l_0/v_0 , and density in units of ρ_0 .

For the purpose of this paper we have run a numerical simulation of super-sonic, super-Alfvénic and self-gravitating MHD turbulence, by solving numerically the equations above, in a 128^3 mesh. The initial density and magnetic fields are uniform; the initial velocity is random, generated in Fourier space with power only on the large scale. We also apply an external random force, to drive the turbulence at a roughly constant rms Mach number of the flow. This force is generated in Fourier space, with power only on small wave numbers ($1 < k < 2$), as the initial velocity.

We let the flow evolve for one dynamical time, defined as $t_{dyn} = L_0/\sigma_v$, where L is the linear size of the computational box, and σ_v is the rms flow velocity. A self-gravitating flow is never statistically relaxed. First a number of collapsing and accreting cores is generated, and later the cores begin to merge. The numerical resolution (128^3 numerical mesh) allows only the description of the initial phase of the collapse of single cores. Results are progressively inaccurate at later times, when the numerical resolution cannot cope with the exceedingly high density. We therefore interrupt the simulation at a time when most cores are just recently formed and start to collapse, which is about one dynamical time of the large scale.

Periodic boundary conditions and large scale external forcing are justified by the fact that we simulate a region of turbulent flow inside a larger turbulent molecular cloud. The rms Mach number of the flow is $\mathcal{M}_s \approx 11$, which corresponds to a linear size $L_0 \approx 6.25$ pc, and an average gas density $\langle n \rangle \approx 320 \text{ cm}^{-3}$, using empirical Larson type relations (Larson 1981). The average magnetic field in this model is rather weak, as justified by our previous work (Padoan & Nordlund 1997, 1999), and such that the average magnetic energy is approximately twice the thermal energy. Assuming a kinetic temperature $T = 10$ K, the rms flow velocity is $\sigma_v = 3.0$ km/s; the average magnetic field strength is $\langle B \rangle = 3.3 \mu\text{G}$, while $\langle B^2 \rangle^{1/2} = 7.1 \mu\text{G}$. Despite this low value of $\langle B \rangle$, strongly magnetized cores are formed by the process of turbulent fragmentation (the maximum field strength in the simulation is $127.8 \mu\text{G}$), due to compressions and stretching in the turbulent flow.

3. Polarized Thermal Dust Emission

We compute the polarized thermal dust emission from the MHD model following the formalism in Fiege & Pudritz (2000) (see also Wardle & Königl 1990). As in Fiege & Pudritz (2000) we are interested in the thermal dust emission at sub-mm wavelengths, and therefore the effect of self-absorption (Hildebrand et al. 1999) and scattering (Novak et al. 1989) can be neglected. We further assume that the grain properties are

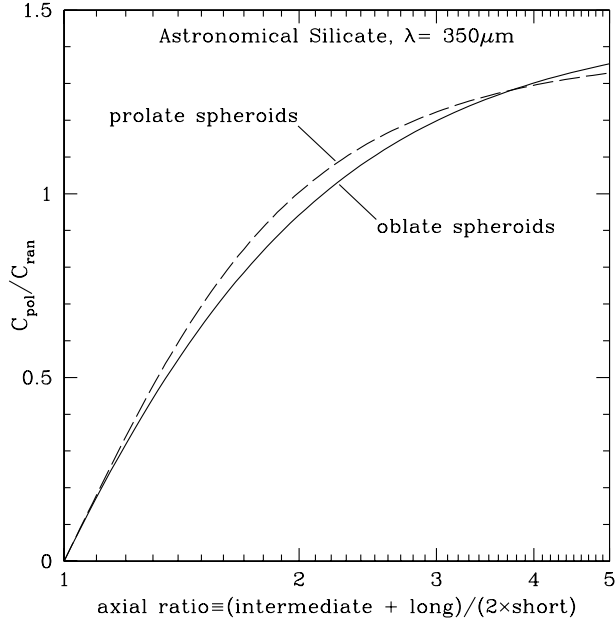


Fig. 1.— Grain cross section ratio as a function of grain axial ratio for prolate spheroids (dashed line) and oblate spheroids (solid line), at wavelength $\lambda = 350 \mu\text{m}$. The grains are the “astronomical silicate” discussed by Draine & Lee (1984), as modified by Li & Draine (2001).

constant² and the temperature is uniform. With these assumptions, the Stokes parameters Q and U are proportional to the following integrals along the line of sight:

$$q = \int \rho \cos 2\psi \cos^2 \gamma ds, \quad (8)$$

$$u = \int \rho \sin 2\psi \cos^2 \gamma ds, \quad (9)$$

where ρ is the gas density, ψ the angle between the projection of \mathbf{B} on the plane of the sky and the North, γ the angle between the local \mathbf{B} vector and the plane of the sky. The polarization angle χ is then given by:

$$\tan 2\chi = \frac{u}{q}. \quad (10)$$

The degree of polarization P , defined as

$$P = \frac{\sqrt{Q^2 + U^2}}{I}, \quad (11)$$

where I is the intensity, is given by:

$$P = \alpha \frac{\sqrt{q^2 + u^2}}{\Sigma - \alpha \Sigma_2}, \quad (12)$$

²Fiege and Pudritz (2000) consider explicitly the contributions to the polarized emission from several grain species, which is not required here since we do not specify any particular set of grain properties.

with

$$\Sigma = \int \rho \, ds, \quad (13)$$

and

$$\Sigma_2 = \frac{1}{2} \int \rho (\cos^2 \gamma - 2/3) \, ds, \quad (14)$$

The coefficient α in equation (12) is defined as

$$\alpha = R F \frac{C_{pol}}{C_{ran}}, \quad (15)$$

where R , F , C_{pol} and C_{ran} are defined by Lee & Draine (1985). C_{pol} is the grain polarization cross section, which differs for oblate spheroids,

$$C_{pol} = C_{\perp} - C_{\parallel}, \quad (16)$$

and prolate spheroids.

$$C_{pol} = (C_{\parallel} - C_{\perp})/2, \quad (17)$$

where C_{\parallel} and C_{\perp} are the polarization cross sections for electric field parallel and perpendicular to the symmetry axis of the grain. C_{ran} is the average cross section for randomly oriented grains,

$$C_{ran} = (2C_{\perp} + C_{\parallel})/3. \quad (18)$$

R is the Rayleigh polarization reduction factor due to imperfect grain alignment, and F the polarization reduction factor due to the turbulent component of the magnetic field. In our case $F = 1$ because the three dimensional magnetic field is provided by the MHD model (assuming that no small scale structure is unresolved in the numerical solution). However, in this work we do not attempt to use specific models for the grain cross sections and for the reduction factors, since our aim is to investigate the effect of the magnetic field topology. We therefore adopt a constant value of $\alpha = 0.15$, which is equivalent to assuming a reasonable value for the maximum degree of polarization, $P_{max} = 15\%$, since

$$P_{max} = \frac{\alpha}{1 - \alpha/6}. \quad (19)$$

In Figure 1 we have plotted C_{pol}/C_{ran} of astronomical silicate spheroids, for “perfect spinning alignment”, as a function of the “axial ratio”, defined as $(a + b)/(2c)$, where a , b and c are the long, intermediate and short axis respectively. For prolate spheroids $b = c$; for oblate spheroids $a = b$. With this definition, the ratio C_{pol}/C_{ran} is nearly the same, at given “axial ratio”, for prolate and oblate spheroids. The astronomical silicate is that discussed by Draine & Lee (1984), as modified by Li & Draine (2001). For wavelengths λ in the range $100 \mu\text{m} < \lambda < 1 \text{mm}$, C_{pol}/C_{ran} is almost independent of λ . Figure 1 is computed for $\lambda = 350 \mu\text{m}$. The adopted value of $\alpha = 0.15$ would require only moderate deviations from sphericity, provided the degree of alignment R is reasonably high. If for example $R \approx 0.33$, a reasonable value of approximately 1.3 for the axial ratio gives the assumed value of α .

We have computed polarization maps from the MHD model in two cases. In the first case, or model *A*, it is assumed that grains are aligned independently of their visual extinction, A_V ; in the second case, or model *B*, it is assumed that grains are not aligned at visual extinction larger than $A_{V,0} = 3 \text{mag}$. The intensity of the radiation field was computed with a Monte Carlo method. Photon packages were sent into the cloud from the background and the scatterings and absorption processes were simulated. In each cell the number of incoming photons was registered and the intensity relative to the background was used to

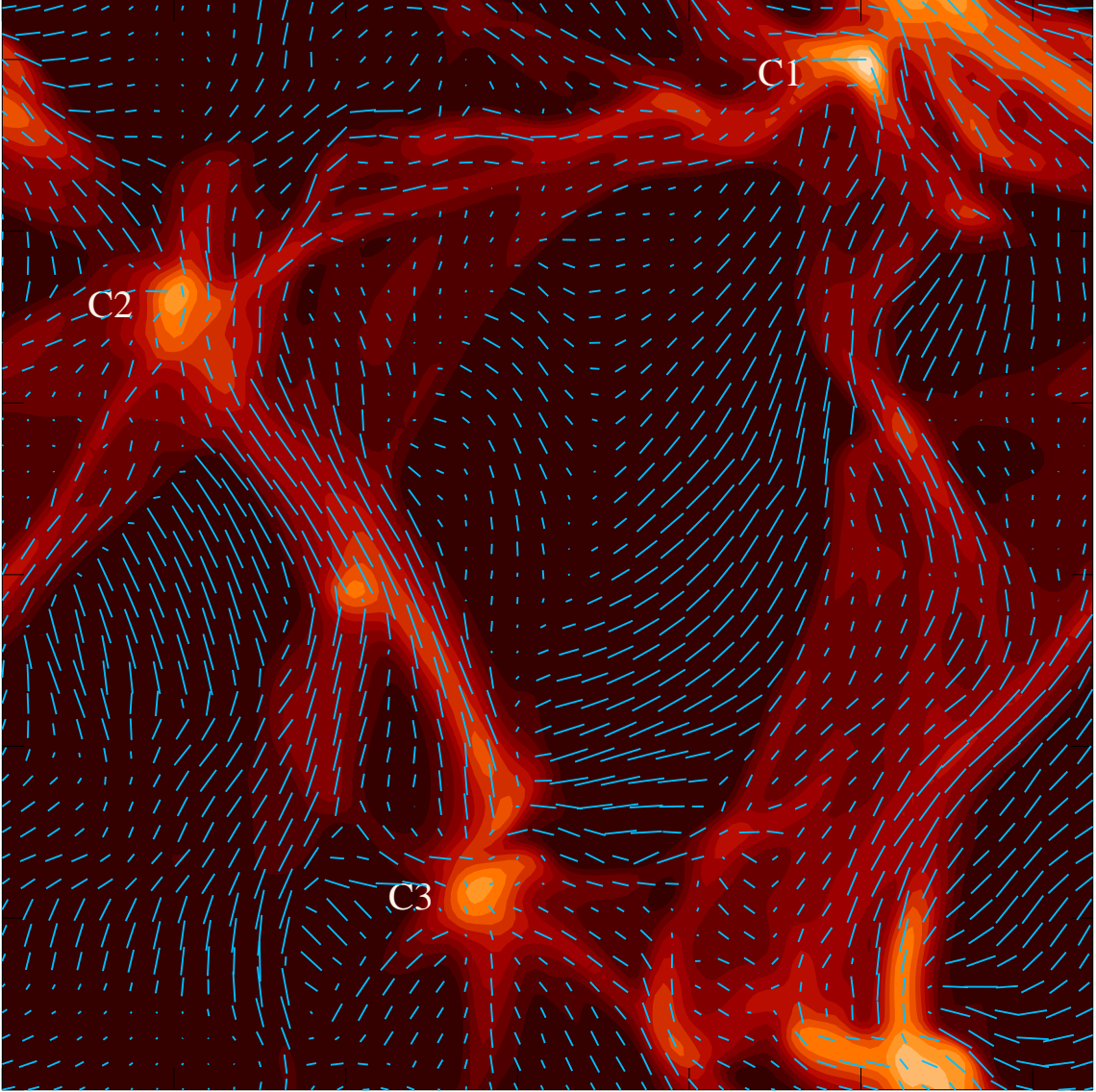


Fig. 2.— Polarization map from the MHD model (model *A*). The length of the polarization vectors is proportional to the degree of polarization, with the longest vector corresponding to $P = 14\%$. Only one polarization vector every three computational cells is plotted. The contour map shows the sub-mm dust continuum intensity I . The position of the self-gravitating cores C1, C2 and C3 (see text in §4) is also shown.

compute the effective values of A_V . The dust opacity was calculated from the relation between $N(\text{H}_2)$ and A_V as given by Bohlin, Savage & Drake (1978). The albedo of the grains was 0.5 and the asymmetry factor of the scattering $g=0.6$.

The polarization maps are plotted in Figure 2 for both model *A* and in Figure 3 for model *B*. The average magnetic field (volume-average over the whole computational box) is oriented in the vertical direction. The length of the polarization vectors is proportional to the degree of polarization, with the

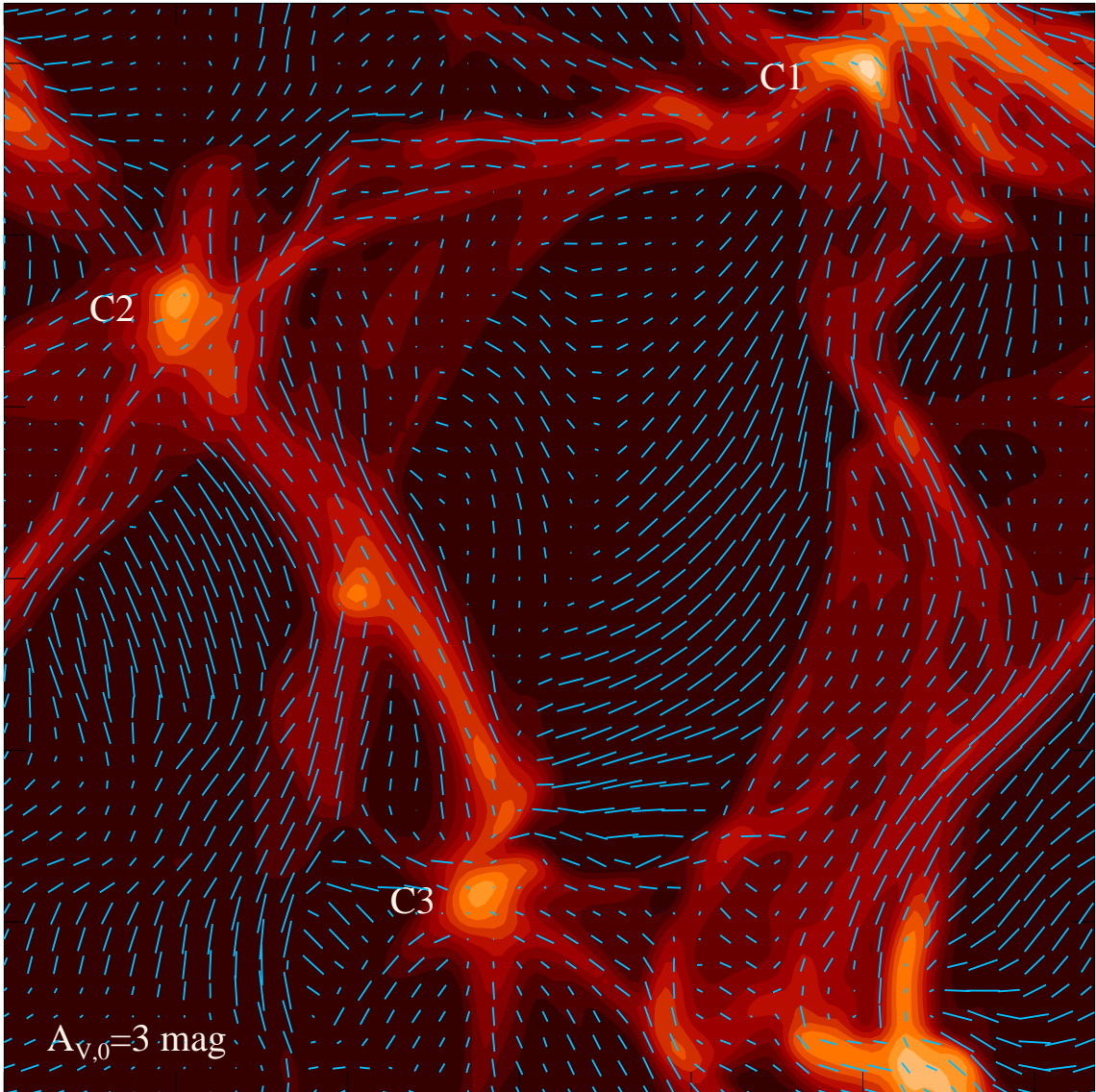


Fig. 3.— As in Figure 1, but assuming unaligned grains above $A_{V,0} = 3$ mag (model *B*).

longest vector corresponding to $P = 14$ %. The contour map shows the sub-mm dust continuum intensity I . Model *B* shows systematically low values of the degree of polarization P in the brightest regions, because at $A_V > 3$ mag the dust contributes to the total flux, but not to the polarized flux (P is defined as the ratio of polarized and total flux). This does not happen in model *A*, with the exception of one region (core C3).

There is no obvious correlation between P and I over the entire map, as shown in the scatter plots of Figure 4. P spans a range of values $0.3\% < P < 14\%$, with $\langle P \rangle = 5.6\%$. Such relatively large values of P , comparable to typically observed values, are usually found in models of super-Alfvénic turbulence. This is due to the fact that each line of sight is normally dominated by one particular dense filament (or edge-on sheet), where the magnetic field is rather uniform because it is amplified in the directions perpendicular to the shock compression that generates that filament (or sheet). The power spectrum of turbulence contains

most of the energy on the largest scales, which constrains the magnetic field tangling, in the sense that the number of correlation lengths of the magnetic field can never be $\gg 1$ (see the discussion in § 7).

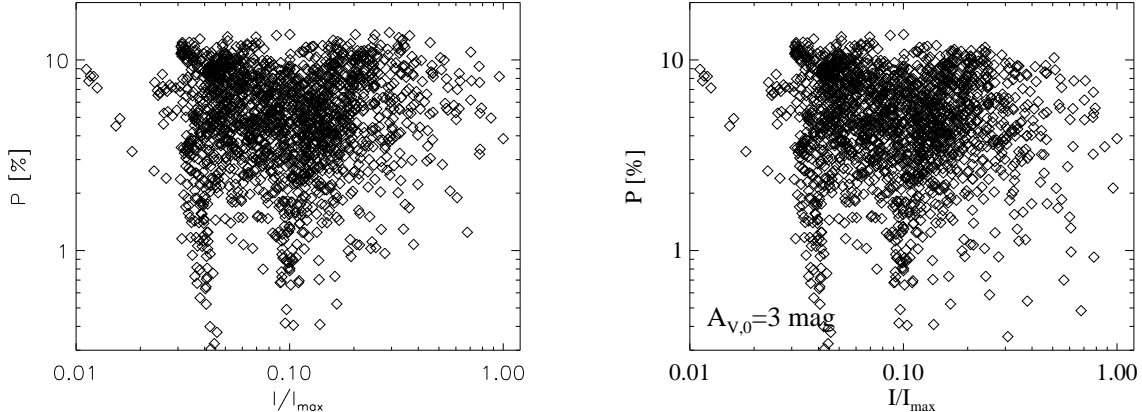


Fig. 4.— Left panel: Scatter plot of the degree of polarization versus the emission intensity from the entire map in Figure 2. Only the polarization vectors shown in Figure 2 are used, that is one position every three computational cells. The average degree of polarization is $\langle P \rangle = 5.6\%$. Right panel: As left panel, but from the entire map in Figure 3, that is with unaligned grains above $A_{V,0} = 3$ mag.

4. Self-Gravitating Cores

For our polarization study, we select the brightest cores in the intensity map shown in Figure 2, in a similar way as protostellar cores would be selected from a sub-mm dust continuum map. Since we are interested in relating the observable properties of the cores with their intrinsic three dimensional structure, we have limited our selection to intensity maxima that are also well defined in the three dimensional MHD data-cube. We have excluded the remaining two or three bright cores that are not easily identified in the original three dimensional data-cube, because of the contribution of multiple structures along the line of sight.

We have selected three cores that we call C1, C2 and C3. Their position is shown on the maps in Figures 2 and 3. We have verified, using the MHD data-cube, that the cores C1, C2 and C3 are gravitationally bound (gravitational energy in excess of the kinetic energy of turbulence). While the core C1 is still being assembled by a turbulent shock (this is also indicated by its position as a density peak in a strongly curved segment of a filament), the core C3 is collapsing with a surrounding flow characterized by accretion along numerous filaments converging towards the core. The magnetic field around the core is roughly aligned with these accretion filaments. In the core C1 the magnetic field is roughly aligned with the filament where the core is located (it is amplified in that direction by the shock compression), and is therefore strongly curved inside the core. The core C2 seems to be an intermediate case between C1 and C3.

The collapsing/accreting configuration of the core C3 can be explained as follows. Once a core is formed by a shock as a density peak along a filament (or on a sheet), part of the gas is moving along the filament (or on the sheet) away from the core, because of the pressure gradient. However, as long as the

core becomes massive enough, its gravitational force becomes larger than the pressure gradient and the flow along the filament is reversed back into the core. In the simple case of a single shock the collapsing core will be accreting along two filaments (the two sides of the original filament), while in the case of the brightest cores, located at the intersection of a number of shocks, many accreting filaments can be found.

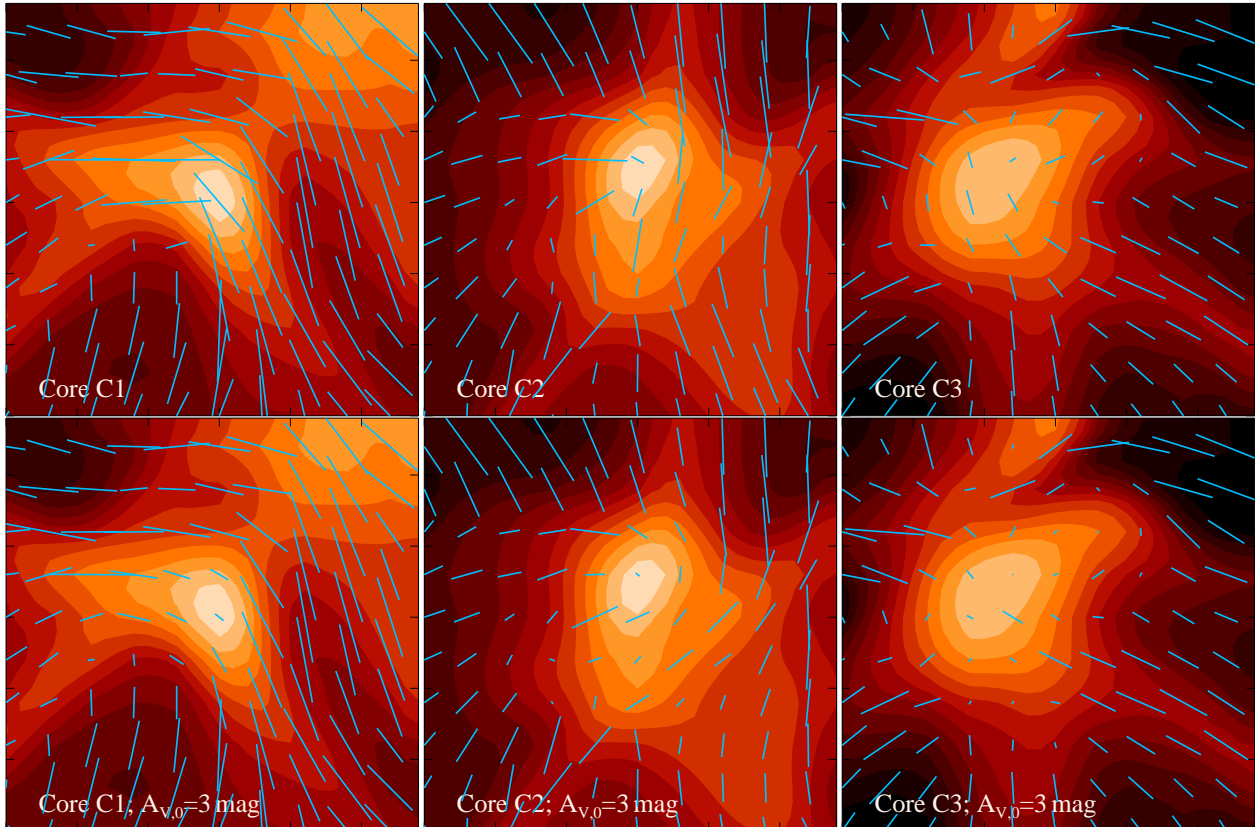


Fig. 5.— Upper panels: Polarization maps as in Figure 2, but limited to the regions around the cores C1, C2 and C3 (see text). The polarization vectors are here plotted for one position every two computational cells, and the largest polarization vectors (found in the core C1) corresponds to $P \approx 11.5\%$. Lower panels: As upper panels, but from the map in Figure 3, that is with unaligned grains above $A_{V,0} = 3$ mag.

The region of the polarization map around each core is shown in the upper panels of Figure 5 for model A. The polarization vectors are here plotted for one position every two computational cells, and the largest polarization vectors (found in the core C1) corresponds to $P \approx 11.5\%$. The respective scatter plots of P versus I (also for model A) are shown in the left panels of Figure 6, where the intensity I is plotted in linear units, for a more direct comparison with published observational plots. The difference in the $P-I$ plot between the cores C1 and C3 is remarkable in model A. The plot for the core C1 is characterized by a lower envelope with P increasing with increasing I , while the plot for the core C3 shows a very clear upper envelope with P decreasing with increasing I . The excursion of the values of P on the envelopes is from approximately 2% to 9% in the first case and from approximately 8% to 2% in the second case. The plot for the core C2 looks like an intermediate case.

Should we conclude that the $P-I$ plot is a diagnostic for the time evolution of a core, from an early

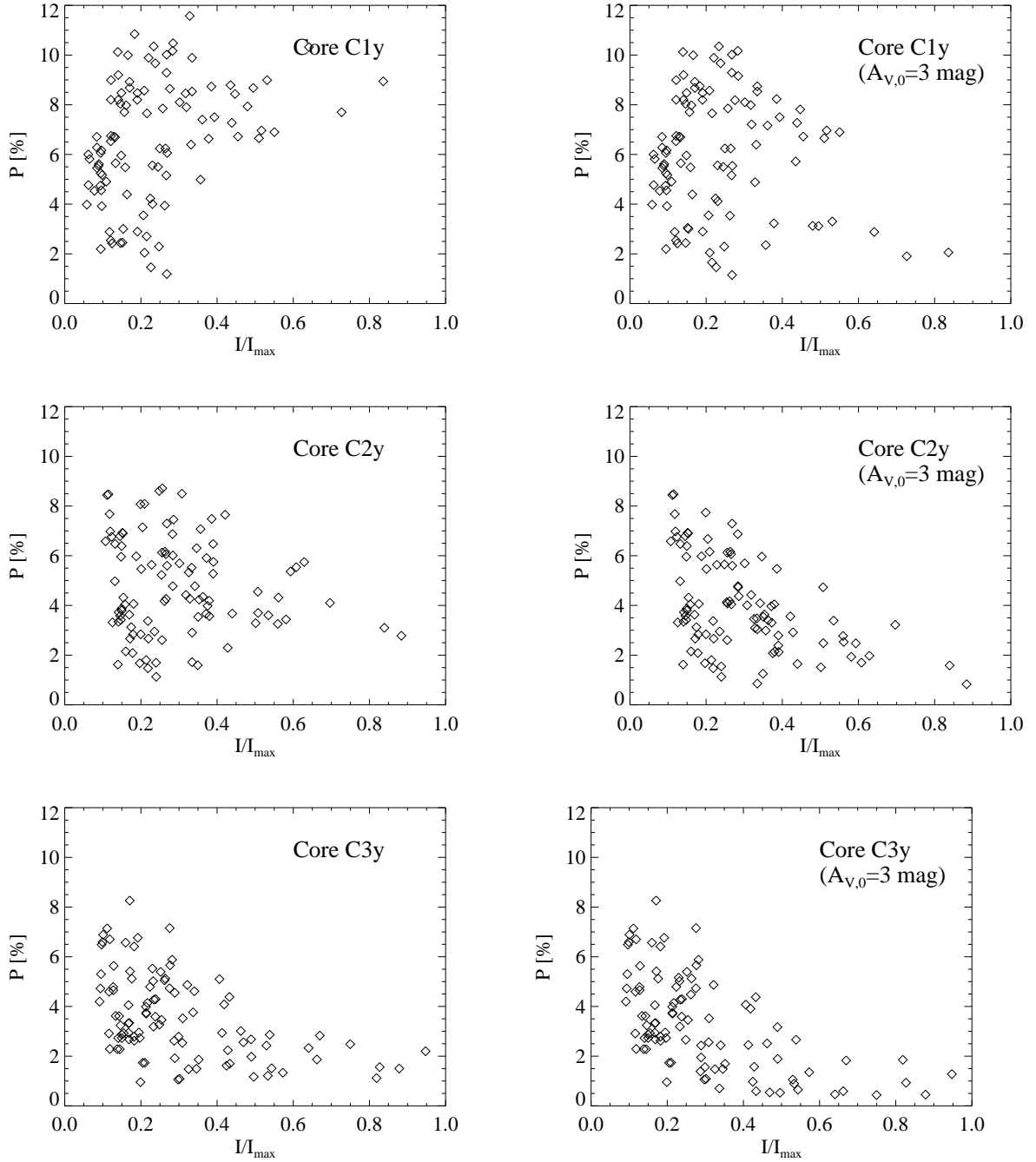


Fig. 6.— Left panels (model *A*): Scatter plots of the degree of polarization versus the emission intensity from the maps in Figure 5 (upper panels). Only the polarization vectors shown in Figure 5 are used, that is one position every two computational cells. Right panels (model *B*): same as left panels, but from the maps in the lower panels of Figure 5, that is assuming unaligned grains above $A_{V,0} = 3$ mag.

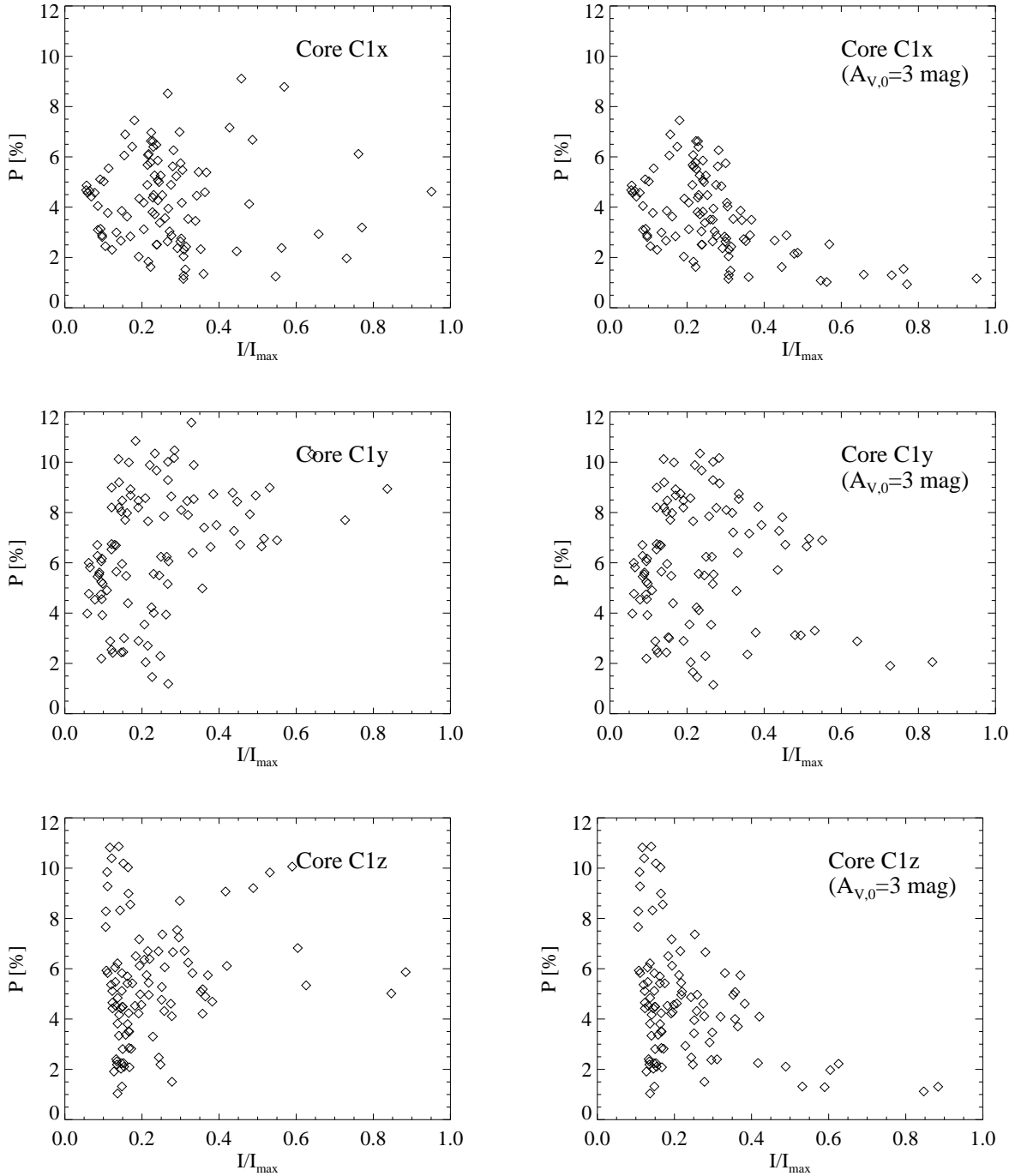


Fig. 7.— Left panel (model A): Scatter plot of the degree of polarization versus the emission intensity for the core C1, seen from three orthogonal points of view. Right panels (model B): same as left panels, but with unaligned grains above $A_{V,0} = 3$ mag.

shock phase to a *collapse phase*? The integration of the Stokes parameters along different lines of sight shows that the P – I plot of the core C3 depends on the direction of the line of sight. Along certain directions P and I are virtually uncorrelated; along others P decreases with increasing I because the magnetic field is roughly parallel to the line of sight towards the center of the core, or because of a cancellation effect due to the direction of polarization within material in front of the core. The P – I plot is therefore sensitive to the viewing angle, and is not a diagnostic for the evolutionary state of the cores (at least with the present numerical resolution that allows only the description of the very early phase of the core collapse).

The situation is different when grains are assumed to be aligned only at visual extinction below $A_{V,0} = 3$ mag, as in model B . The polarization maps of the cores in the case of model B are shown in the lower panels of Figure 5, and the corresponding P – I plots in the right panels of Figure 6. The upper envelope in the P – I plot, with P decreasing with increasing I , is always found, since at visual extinction above $A_{V,0} = 3$ mag the dust contributes to the continuum intensity I , but not to the polarized flux (P is defined as the ratio of polarized and total flux –eq. (11)). The direction of polarization is also affected by the lack of alignment of grains at large visual extinction. As an example, the region at the south of the core C2 shows a magnetic field direction roughly parallel to the elongation of the core in model A , while the magnetic field direction is almost perpendicular to the core elongation in model B .

Figure 7 shows the P – I plots for the core C1 seen from three different orthogonal directions, in model A (left panels) and B (right panels). These plots show that P always decreases with increasing I in model B , independent of the viewing angle.

The histograms of the polarization angle χ in the maps of Figure 5 are plotted in Figure 8. For computing these histograms we have used all the polarization vectors available, that is one per computational cell. Since the maps are made of 20×20 pixels, we have used 400 polarization vectors for each histogram, while in Figures 4 and 5 only $10 \times 10 = 100$ vectors were used for clarity. The plots in Figure 7 show very broad distributions of χ . The values of χ are limited to the interval $[-\pi/2, \pi/2]$, but the reference direction, or the origin of the interval, can be shifted arbitrarily by an amount between 0 and π . We have done so in order to minimize the dispersion of χ , which is obtained by shifting the origin of the angle to the approximate location of the minimum in the histogram. In this way the dispersion σ_χ has a robust physical meaning, independent of the particular local orientation of the average magnetic field relative to the North. No Gaussian fit of the histogram is attempted, and σ_χ is simply defined as

$$\sigma_\chi = \langle (\chi - \langle \chi \rangle)^2 \rangle^{1/2} \quad (20)$$

with the values of χ defined in the interval that minimizes this expression, as explained above. Differences between models A and B are rather small. Results are listed Table 1. For both models A and B we find the average value of the rms χ to be $\sigma_\chi = 0.60 \pm 0.11$.

5. Observational P – I Plots of “Quiescent” Cores

In this work we define as “quiescent” any starless or low mass star forming core. We do not try to model regions of massive star formation, where the enhanced radiation field must have a considerable effect on the grain alignment (Draine & Weingartner 1996, 1997).

A number of recent sub-mm polarization maps of quiescent cores can be used to study the correlation of the degree of polarization P and the sub-mm dust continuum intensity I . Davis et al. (2000) observed the Serpens low mass star forming region, which contains eight cores. Polarization maps of the three cores

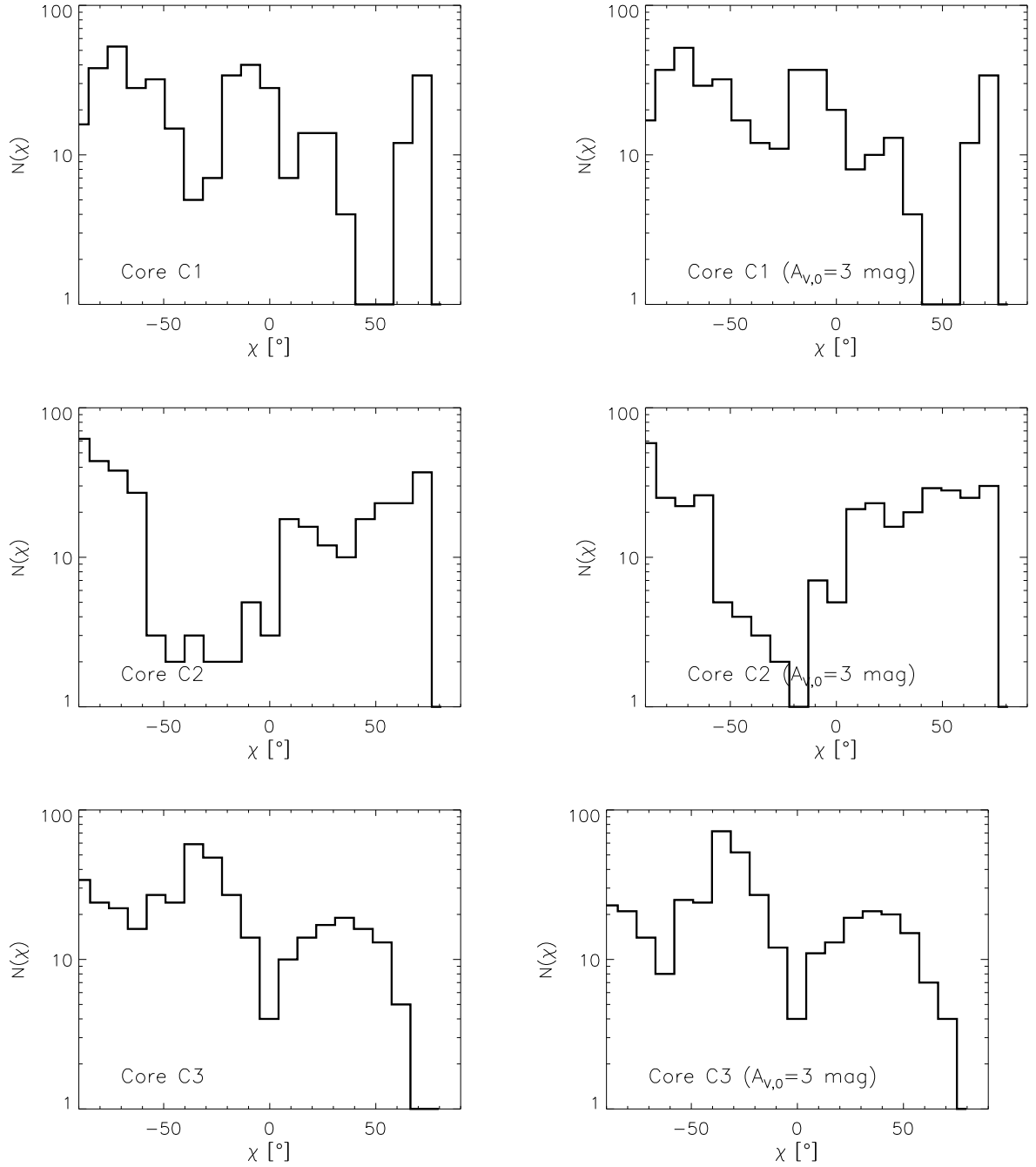


Fig. 8.— Left panels (model A): Histograms of the polarization angle χ from the polarization maps shown in Figure 5 (upper panels). All the available polarization vectors have been used, that is one per computational cell. Right panels (model B): same as left panels, but from the polarization maps in the lower panels of Figure 5, that is with unaligned grains above $A_{V,0} = 3$ mag.

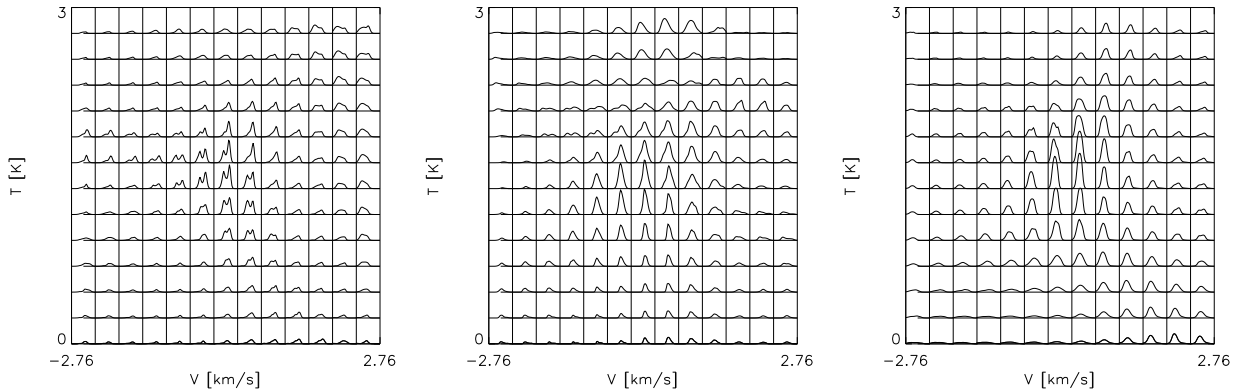


Fig. 9.— Spectral maps of the J=1–0 transition of CS. The maps are located around the cores C1, C2 and C3, from top to bottom respectively. The regions shown in the maps correspond to the regions included in the maps of Figure 5. The velocity axis ranges from -2.76 to 2.76 km/s, and the antenna temperature axis from 0 to 3 K.

L1544, L183 and L43 were obtained by Ward–Thompson et al. (2000) and three more cores, CB 26, CB 24 and DC 253-1.6 (CG 30) were mapped by Henning et al. (2001). All these regions were observed at $850 \mu\text{m}$, with the SCUBA bolometer array at the James Clerk Maxwell Telescope. In all of the 14 cores the value of P is found to decrease rather steeply with increasing I . Polarization vectors from the lower intensity regions around the cores are always much larger than the vectors close to the center of the cores.

P – I plots are presented both in Davis et al. (2000) and in Henning et al. (2001). They are very similar to the P – I plots from our model B , presented in the previous section. The upper envelope of the plots is defined by values of P from 1-2% at the highest I , to 8-10% at the lowest values of I . The drop in P is roughly consistent with a constant polarized flux, where the polarized flux is defined as $P \times I$. This suggests that a significant fraction of the dust emission is from grains that do not contribute significantly to the polarization, presumably unaligned grains.

Model A cannot reproduce the same result for all cores, but only in some cases due to the fortuitous orientation of the magnetic field or to a cancellation effect also dependent on the orientation of the core relative to the line of sight. It is possible that a numerical simulation with higher resolution, able to follow the collapse of cores to larger densities, may generate a stronger cancellation effect. The gravitational collapse is expected to drag the lines of force of the magnetic field towards the core center, which could generate a cancellation effect. However, it is not clear how important this effect may be, once diluted over the size of the telescope beam. It is also difficult to imagine it should be independent of orientation, since the average magnetic field before the collapse defines a specific direction.

6. Distribution of Polarization Angle and Magnetic Field Strength

In linear transverse oscillations of a line of force (for example Alfvén waves in a uniform medium) the ratio of the lateral and transverse velocities is equal to the deviation of the line of force from a straight line. This deviation of the field from a straight line is measured by the angle χ between the straight line and the local line of force. If the transverse velocity is the Alfvén velocity v_a , and the lateral velocity is the rms

turbulent velocity σ_v , then

$$\sigma_\chi \approx \frac{\sigma_v}{v_a} \equiv \mathcal{M}_a, \quad (21)$$

where \mathcal{M}_a is the Alfvénic Mach number. This is strictly valid only in linear theory. We can define a coefficient f that quantifies the deviation from the prediction of the linear theory:

$$f \equiv \frac{\langle v_a^2 \rangle^{1/2}}{\sigma_v / \sigma_\chi} = \frac{\langle B^2 / (4\pi\rho) \rangle^{1/2}}{\sigma_v / \sigma_\chi}, \quad (22)$$

where the numerator is the rms Alfvén velocity, averaged inside the volume under study. Equation (21), or equivalently the value $f = 1$, was first used to derive the magnetic field strength in the Galaxy by Davis (1951) and Chandrasekhar and Fermi (1953). This method was further discussed by Zweibel (1990) and Myers & Goodman (1991). It has also been tested on the results of MHD simulations of sub-Alfvénic turbulence by Ostriker, Stone & Gammie (2001). They find that for small dispersion of the polarization angle ($\sigma_\chi < 0.44$ radians) the Chandrasekhar–Fermi formula provides a good estimate of the plane of the sky field strength, if a coefficient $f \approx 0.5$ is used. Similar results are found by Heitsch et al. (2001), using numerical simulations of mildly super-Alfvénic turbulence.

In protostellar cores and Bok globules the dispersion of the polarization angle is sometimes very large, and the Chandrasekhar–Fermi formula is not expected to hold. However, the formula is sometimes applied irrespective of the large value of σ_χ (eg Itoh et al. 1999; Davis et al. 2000; Henning et al. 2001). This is perhaps justified by the expectation that the degree of topological complexity of the magnetic field, and so the value of σ_χ , should be related in some way to the rms Alfvénic Mach number \mathcal{M}_a . A full numerical study of the dependence of σ_χ on \mathcal{M}_a can be pursued with the MHD turbulence simulations, and will be presented elsewhere. For the purpose of this work we test the Chandrasekhar–Fermi formula on the cores C1, C2 and C3, and provide the values of the corresponding correction factor f .

The turbulent velocity dispersion in protostellar cores and Bok globules is often estimated using the line width of the CS molecule. It is possible that the bulk of the CS emission come from an envelope around the core, and not from the core interior, where most of the dust emission is generated, at least for the densest cores. This complicates the application of the Chandrasekhar–Fermi formula and its interpretation. For this reason, we have tested the formula by defining the turbulent velocity as given by the CS spectra.

Maps of synthetic spectra of the J=1–0 transition of CS are computed using a non-LTE Monte Carlo radiative transfer code (Juvella 1997, 1998), from the three dimensional density and velocity fields generated in the numerical MHD experiment. The method of computing synthetic spectra was presented in Padoan et al. (1998). We assume a linear size of the computational box $L = 6.25$ pc, a uniform temperature $T = 10$ K, an rms turbulent velocity $\sigma_v = 3.0$ km/s and an average gas density $\langle n \rangle = 320$ cm⁻³. These values are used to scale the numerical variables into physical units. In the radiative transfer computation the full three dimensional density and velocity fields are used. The radiative transfer is a non-local problem, and so it is solved for the whole three dimensional computational box.

Spectral maps are obtained for the same lines of sight that define the polarization maps. The CS spectral maps that match the polarization maps of Figure 5 are plotted in Figure 9. All the spectra are used to compute the rms velocity σ_v . This is defined as the rms velocity averaged along the spectral profile, without any Gaussian fit:

$$\sigma_v = \left(\frac{\int (v - \langle v \rangle)^2 T(v) dv}{\int T(v) dv} \right)^{1/2} \quad (23)$$

where $T(v)$ is the antenna temperature at the velocity channel v , and the result is averaged over the whole

Core	C1			C2			C3		
	x	y	z	x	y	z	x	y	z
σ_v [km/s]	0.96	0.96	0.82	0.94	1.34	1.04	1.00	0.73	1.32
σ_χ [rad]	0.48	0.73	0.37	0.59	0.58	0.71	0.55	0.73	0.65
	(0.49)	(0.70)	(0.37)	(0.64)	(0.62)	(0.71)	(0.52)	(0.74)	(0.65)
f	0.32	0.48	0.29	0.43	0.29	0.46	0.35	0.63	0.31
	(0.32)	(0.46)	(0.29)	(0.46)	(0.31)	(0.46)	(0.33)	(0.64)	(0.31)

Table 1: Estimated parameters for the three cores C1, C2 and C3. From top to bottom: rms turbulent velocity from CS spectral maps; rms polarization angle; correction factor for the Chandrasekhar–Fermi formula (see text). Values in parenthesis are for the case of unaligned grains above $A_{V,0} = 3$ mag.

spectral map of each core. The average velocity $\langle v \rangle$ is defined as

$$\langle v \rangle = \frac{\int v T(v) dv}{\int T(v) dv} \quad (24)$$

The values of σ_v for three orthogonal lines of sight are listed in Table 1. The average value is $\sigma_v = 1.01 \pm 0.19$ km/s.

In order to determine the value of the coefficient f , we finally need to compute the rms Alfvén velocity in the cores. This is done directly in the three dimensional MHD data cube. Using the values of σ_χ computed in the previous section, and the values of σ_v and rms v_a computed here, we can now evaluate the coefficient f . Results are listed in Table 1. The average value of f is found to be $f = 0.40 \pm 0.11$ for both models A and B .

7. Discussion

In order to describe the formation of protostellar cores we have simulated the dynamics of molecular cloud turbulence on a relatively large scale (≈ 6 pc). Simulating a large scale is necessary because the boundary and initial conditions of a numerical simulation (and much more of an analytic model) are always idealized in some way. For example, a numerical simulation or an analytic model describing the evolution and collapse of a single protostellar core can hardly be considered as models for the core *formation*, since the core is obviously formed by the ad hoc setup of the initial conditions. On the other hand, if a larger scale is simulated, the process of core formation is controlled by the gas dynamics on the large scale, and may even be rather insensitive to the specific initial and boundary conditions at the large scale.

In the simulation used for this work the typical size of cores is less than one tenth of the size of the computational box, and so we argue that our periodic boundary conditions do not affect too much the formation and evolution of dense cores. The setup of the initial conditions is also unlikely to affect dramatically the outcome of the simulation, since after one dynamical time the turbulent flow begins to lose memory of its initial conditions. The random external driving force can instead have important effects, in the sense that the flow would develop much more small scale structure if the forcing was done on a small scale, and the number of correlation lengths of the magnetic field, N_{corr} , could be relatively large. However, that would imply a power spectrum of turbulence peaking on small scales. In contrast, all observational evidence for the power spectrum of turbulence in molecular clouds is consistent with a scale free dynamics (Miesch & Bally 1994; Ossenkopf & Mac Low 2000), with most energy on the largest scale. The large scale

driving used in the present simulation, is therefore consistent with the observations. As a consequence, the number of correlation lengths of the magnetic field must be relatively small, $N_{corr} \sim 1$. This explains the relatively large values of P found from our super-Alfvénic simulations, since a significant cancellation effect requires both a weak magnetic field (super-Alfvénic turbulence) and a large number of correlation lengths.

It is well established that the polarized extinction of background stars at optical and near-IR wavelengths does not reveal the magnetic field direction in the dense interiors of molecular clouds, beyond an optical depth $A_v = 1 - 2$ mag (Goodman et al. 1995; Arce et al. 1998). This is generally interpreted as the effect of unaligned grains at large visual extinction, since it can be shown that most alignment mechanisms are ineffective at large optical depth (Lazarian, Goodman & Myers 1997). Wiebe & Watson (2001), on the contrary, suggest that the results of polarization studies of background stars can be explained by a cancellation effect due to the magnetic field tangling along the line of sight. This requires super-Alfvénic turbulence and a large number of correlation lengths of the magnetic field, N_{corr} . They find that $N_{corr} \geq 10$ is necessary to explain the observations, and use a numerical MHD simulation by Stone, Ostriker & Gammie (1998) as an example of a theoretical model with $N_{corr} > 10$. However, as explained in the previous paragraph, there is no observational evidence in favor of a power spectrum of turbulence with a peak at small scale, which is needed to produce a large value of N_{corr} . The simulation by Stone, Ostriker & Gammie (1998) used by Wiebe and Watson (2001) is performed with a random driving on an intermediate scale, which explains the large value of N_{corr} , but is certainly not motivated by the observations.

In § 5 we have seen that recent sub-mm polarization maps of quiescent cores always produce $P-I$ plots characterized by an upper envelope with P decreasing with increasing I . This result is predicted by our model B , that is by assuming that grains at visual extinction larger than $A_{V,0} = 3$ mag are not aligned. It is not reproduced by model A , where the grain alignment is assumed to be independent of A_V , because the magnetic field tangling in the cores is insufficient to produce such drop in P . Although it is still possible that higher resolution simulations following the core collapse to higher densities generate a larger cancellation effect, that remains to be proven. From the present calculations it seems that the reasonable assumptions of model B provide a good interpretation of the observational $P-I$ plots. If this interpretation is correct, we can conclude that sub-mm polarization maps cannot probe the magnetic field structure inside quiescent cores, at visual extinction larger than $A_{V,0} = 3$ mag. The use of such maps to constrain models of protostellar core formation and evolution is therefore questionable, especially if the effect of unaligned grains is not taken carefully into account. Polarization studies of sub-mm dust continuum emission from quiescent cores are therefore not inconsistent with previous results of polarized extinction of background stars at optical and near-IR wavelengths mentioned above.

The specific value of $A_{V,0} = 3$ mag used to compute model B is a “conservative” choice. A value of $A_{V,0} \approx 2$ mag, or even lower, is not ruled out by our study. It is likely that the alignment efficiency of grains begins to decrease significantly at $A_V = 1 - 2$ mag, as suggested by theoretical studies (Lazarian, Goodman & Myers 1997). In this work we show that at values of visual extinction larger than 3 mag grains must be almost completely unaligned.

The MHD simulation used in this work has a limited numerical resolution. A 128^3 numerical mesh has been used and the volume selected around each core contains only 20^3 computational cells. Differences in the polarization maps of the cores between models A and B (see Figure 5) are equally limited. A much higher numerical resolution could in principle generate even larger differences between the magnetic field orientation in the densest regions of the cores and in their lower density envelopes. The center of the core at $A_V > 3$ mag, for example, could have collapsed dragging in the magnetic field lines, and this process would be totally invisible in the polarization maps. However, models for the formation and evolution of

protostellar cores could be tested with polarization maps of quiescent cores if the comparison were limited to the regions of low visual extinction around the cores.

We have shown in the previous section that the Chandrasekhar–Fermi formula predicts the value of the rms Alfvén speed in the cores, if a correction factor $f \approx 0.4$ is used, and if the rms turbulent velocity is derived from the line width of the J=1–0 CS transition. The value of σ_χ should be appropriately minimized as discussed in the previous section. However, in order to infer a magnetic field strength from an rms Alfvén speed and σ_χ , the gas density in the cores must be estimated, which introduces a significant uncertainty.

8. Conclusions

In this work we have computed dust continuum polarization from protostellar cores, assembled by super-sonic turbulent flows in models of molecular clouds, using numerical simulations of highly super-sonic MHD turbulence. The results are compared with recent polarization maps of quiescent protostellar cores and Bok globules.

The main results of this work are: i) Values of P between 1 and 10% (up to almost P_{max}) are produced by super-Alfvénic turbulence; ii) A steep decrease of P with increasing I , as observed in a number of protostellar cores and Bok globules, is always found in self-gravitating cores selected from the MHD simulation, if grains are not aligned above a certain value of visual extinction $A_{V,0}$ (model B); iii) The same behavior is hard to reproduce if dust grains are aligned independently of A_V (model A); iv) The Chandrasekhar–Fermi formula, corrected by a factor $f \approx 0.4$, can be used to estimate the average magnetic field strength in the cores.

We conclude that sub-mm polarization maps of quiescent cores are not likely to faithfully map the magnetic field inside the cores at visual extinction larger than $A_{V,0} \approx 3$ mag. The use of such maps to constrain models of protostellar core formation and evolution is questionable, especially if the effect of unaligned grains is not properly taken into account. This conclusion shows that there is no inconsistency between the results from optical and near-IR polarized absorption of background stars, and the observed polarization of sub-mm dust continuum from quiescent cores. In both cases, grains at large visual extinction appear to be virtually unaligned.

This work was supported by NSF grant AST-9721455. Åke Nordlund acknowledges partial support by the Danish National Research Foundation through its establishment of the Theoretical Astrophysics Center. Mika Juvela acknowledges support by the Academy of Finland Grant no. 1011055.

References

- Arce, H. G., Goodman, A. A., Bastien, P., Manset, N., Sumner, M. 1998, ApJ, 499, L93
- Bohlin, R. C., Savage, B. D., Drake, J. F. 1978, ApJ, 224, 132
- Chandrasekhar, S., Fermi, E. 1953, ApJ, 118, 113
- Clemens, D. P., Bookbinder, J., Goodman, A., Kristen, H., Myers, P., Padoan, P., Wood, K., Heyer, M. H., Heiles, C., Jones, T. J., Dickey, J., Young, E., Rieke, G., Dow, K., Dowell, C. D., Draine, B., Greaves,

- J., Klaas, U., Laureijs, R., Lazarian, A., Shulz, B., Zweibel, E. 2000, in American Astronomical Society Meeting, Vol. 196, 2508
- Coppin, K. E. K., Greaves, J. S., Jenness, T., Holland, W. S. 2000, *A&A*, 356, 1031
- Davis, C. J., Chrysostomou, A., Matthews, H. E., Jenness, T., Ray, T. P. 2000, *ApJ*, 530, L115
- Davis, L. 1951, *Phys. Rev.*, 81, 890
- Draine, B. T., Lee, H. M. 1984, *ApJ*, 285, 89
- Draine, B. T., Weingartner, J. C. 1996, *ApJ*, 470, 551
- Draine, B. T., Weingartner, J. C. 1997, *ApJ*, 480, 633
- Fiege, J. D., Pudritz, R. E. 2000, *ApJ*, 544, 830
- Gerakines, P. A., Whittet, D. C. B., Lazarian, A. 1995, *ApJ*, 455, L171
- Glenn, J., Walker, C. K., Young, E. T. 1999, *ApJ*, 511, 812
- Goodman, A. A., Jones, T. J., Lada, E. A., Myers, P. C. 1995, *ApJ*, 448, 748
- Greaves, J. S., Holland, W. S., Minchin, N. R., Murray, A. G., Stevens, J. A. 1999, *A&A*, 344, 668
- Heitsch, F., Zweibel, E., Mac Low, M. M., Li, P. S., Norman, M. L. 2001, *astro-ph/0103286*
- Henning, T. 2001, *ApJ*, submitted
- Hildebrand, R. H., Dotson, J. L., Dowell, C. D., Schleuning, D. A., Vaillancourt, J. E. 1999, *ApJ*, 516, 834
- Itoh, Y., Chrysostomou, A., Burton, M., Hough, J. H., Tamura, M. 1999, *MNRAS*, 304, 406
- Juvela, M. 1997, *A&A*, 322, 943
- Juvela, M. 1998, *A&A*, 338, 723
- Larson, R. B. 1981, *MNRAS*, 194, 809
- Lazarian, A., Goodman, A. A., Myers, P. C. 1997, *ApJ*, 490, 273
- Lee, H. M., Draine, B. T. 1985, *ApJ*, 290, 211
- Li, A., Draine, B. T. 2001, *ApJ*, 553, (in press)
- Matthews, B. C., Wilson, C. D. 2000, *ApJ*, 531, 868
- Miesch, M. S., Bally, J. 1994, *ApJ*, 429, 645
- Minchin, N. R., Bonifacio, V. H. R., Murray, A. G. 1996, *A&A*, 315, L5
- Myers, P. C., Goodman, A. A. 1991, *ApJ*, 373, 509
- Novak, G., Gonatas, D. P., Hildebrand, R. H., Platt, S. R., Dragovan, M. 1989, *ApJ*, 345, 802
- Ossenkopf, V., Mac Low, M. 2000, *astro-ph/0012247*
- Ostriker, E. C., Stone, J. M., Gammie, C. F. 2001, *ApJ*, 546, 980
- Padoan, P., Juvela, M., Bally, J., Nordlund, Å. 1998, *ApJ*, 504, 300

- Padoan, P., Juvela, M., Goodman, A. A., Nordlund, Å. 2001, ApJ, (in press –also astro-ph/0011122)
- Padoan, P., Nordlund, Å. 1997, astro-ph/9706176
- Padoan, P., Nordlund, Å. 1999, ApJ, 526, 279
- Padoan, P., Zweibel, E., Nordlund, Å. 2000, ApJ, 540, 332
- Vallée, J. P., Bastien, P., Greaves, J. S. 2000, ApJ, 542, 352
- Ward-Thompson, D., Kirk, J. M., Crutcher, R. M., Greaves, J. S., Holland, W. S., André, P. 2000, ApJ, 537, L135
- Wardle, M., Konigl, A. 1990, ApJ, 362, 120
- Wiebe, D. S., Watson, W. D. 2001, ApJ, 549, L115
- Zweibel, E. G. 1990, ApJ, 362, 545